ARTICLE

# Optical Frequency Comb-Based Cavity-Enhanced Fourier-Transform Spectroscopy: Application to Collisional Line-Shape Study[†]

Akiko Nishiyama[*‡] Grzegorz Kowzan, Dominik Charczun, Ryszard S. Trawiński, Piotr Masłowski[*]

*Institute of Physics, Faculty of Physics, Astronomy and Informatics, Nicolaus Copernicus University in Toruń, Toruń 87-100, Poland*

(Dated: Received on November 1, 2019; Accepted on November 27, 2019)

Direct-comb spectroscopy techniques uses optical frequency combs (OFCs) as spectroscopic light source. They deliver high sensitivity, high frequency resolution and precision in a broad spectral range. Due to these features, the field has burgeoned in recent years. In this work we constructed an OFC-based cavity-enhanced Fourier-transform spectrometer in the near-infrared region and used it for a line-shape study of rovibrational transitions of CO perturbed by Ar. The highly sensitive measurements spanned the wavenumber range from 6270 $cm^{-1}$ to 6410 $cm^{-1}$, which covered both P and R branch of the second overtone band of CO. The spectrometer delivers high-resolution surpassing the Fourier-transform resolution limit determined by interferogram length, successfully removing ringing and broadening effects caused by instrumental line shape function. The instrumental-line-shape-free method and high signal-to-noise ratio in the measurement allowed us to observe collisional effects beyond those described by the Voigt profile. We retrieved collisional line-shape parameters by fitting the speed-dependent Voigt profile and found good agreement with the values given by precise cavity ring-down spectroscopy measurements that used a continuous-wave laser referenced to a stabilized OFC. The results demonstrate that OFC-based cavity-enhanced Fourier-transform spectroscopy is a strong tool for accurate line-shape studies that will be crucial for future spectral databases.

**Key words:** Carbon monoxide, Spectral lineshapes, Optical frequency comb, Cavity enhanced absorption spectroscopy, Fourier-transform spectroscopy

## I. INTRODUCTION

Optical frequency combs (OFCs) have spectrum consisting of millions of equally spaced narrow modes that can be stabilized to radio frequency (RF) or optical frequency standards. They have been adopted as reliable optical frequency rulers in the fields of metrology and precise spectroscopy [1, 2]. Using OFCs as spectroscopic light sources led to development of such techniques as: virtually-imaged phased-array (VIPA) spectroscopy [3, 4], dual-comb spectroscopy [5–7] and OFC-based Fourier-transform spectroscopy (FTS) [8, 9]. These direct-comb spectroscopy techniques have been intensely developed in recent years because of their high potential for applications in various fields, including high-resolution molecular and atomic spectroscopy [10–13], remote sensing [14], and breath analysis [4]. In direct-comb spectroscopy, it is possible to extract spectral information from a large number of comb modes.

If the comb modes are resolved, then the frequency resolution is determined by comb mode linewidth, which makes it on par with conventional high-resolution spectrometers using continuous wave (cw) lasers. OFCs stabilized to primary frequency standards offer state-of-the-art frequency accuracy and precision that transfers directly to frequency accuracy of direct-comb spectroscopy. Furthermore, thanks to the broadband spectrum of OFCs, spectral acquisition over a wide wavelength range can be performed instantaneously.

Dual-comb spectroscopy needs two OFCs and requires them to be highly phase-stable relative to each other. Alternatively, the intrinsic phase instability can be accounted for in post-processing but this requires sophisticated phase correction algorithms. VIPA spectrometers usually require filtering the OFC to increase comb mode spacing due to insufficient resolution and their bandwidth is strongly limited by the physical size of the photodetector array. In contrast, OFC-based FTS is simple, inexpensive and versatile because it is based on simple Michelson interferometer like in traditional Fourier-transform infrared (FTIR) spectroscopy.

[†]Part of the special topic on "the 3rd Asian Workshop on Molecular Spectroscopy"

[*]Authors to whom correspondence should be addressed. E-mail: akiko@fizyka.umk.pl, pima@fizyka.umk.pl

[‡]JSPS Overseas Research Fellow.

DOI:10.1063/1674-0068/cjcp1911192 

From the principle of Fourier transform, the resolution in traditional FTIR spectroscopy is limited by the maximum delay range ($\Delta_{\max}$) of the interferometer to $c/\Delta_{\max}$. In the case that the resolution is worse than a molecular absorption width, observed spectral line shapes are distorted: the lines are broadened, their amplitudes are changed and ringing is present. These effects occur because the observed spectrum is the convolution of the instrumental line shape (ILS) function with the actual spectrum [15]. The OFC offers significant advantages over the traditional FTIR spectrometer. The OFC-based FTS removes the influence of ILS from resulting spectra and is far beyond the nominal resolution limit [9, 17].

Additionally, the high spectral brightness and coherence of OFC led high signal-to-noise ratios (SNR) in recording times orders of magnitude shorter than that in conventional FTIR. Furthermore, direct-comb spectroscopy can be successfully combined with cavity-enhanced techniques. The enhancement cavity increases the interaction length between the intracavity sample and the resonant light, and provides high detection sensitivity. There have been reports of direct-comb versions of cavity-ring-down spectroscopy (CRDS) [16], cavity-mode width spectroscopy (CMWS), and cavity-mode dispersion spectroscopy (CMDS) [17, 18], however, the most established OFC-based cavity spectroscopy is cavity-enhanced absorption spectroscopy (CEAS) [4, 10, 11, 17, 19–23]. In CEAS the absorption information is determined directly from attenuation of the transmitted light. In OFC-based CEAS, many comb modes in a wide wavelength range are resonant with the cavity and their intensities are detected simultaneously.

Precise spectroscopic line-shape parameters, such as accurate center frequencies or pressure broadening and shift coefficients, are important for a variety of astrophysical and terrestrial atmosphere observations. They are also crucial for verifying intermolecular interaction potentials by comparing *ab intio* line-shape parameters with experimental ones. HITRAN and other databases provide spectroscopic data for many molecules, but the accuracy of the data is in many cases insufficient [24]. Atmospheric CO plays an important role in the carbon cycle [25] and can be a useful probe for astronomical observations [26, 27]. Since CO perturbed by Ar is a relatively simple system, precise line-shape measurements of this system are useful for comparison of the experimental and theoretical line-shape profiles [28–31]. There have been several reports of collisional line-shape parameters of transitions in the fundamental band and the first overtone band of CO perturbed by Ar, but only a few articles reporting the line broadening parameters of the second overtone (0–3) band so far [32–34]. Our group performed precise line-shape measurements of the 0–3 band employing a cw-CRDS spectrometer referenced to an OFC [33], however, since this measurement involved step scanning the spectrum with a cw laser, parameters of only several lines in the P branch were determined.

We measured P and R branch transitions of the 0–3 band of CO perturbed by Ar using an OFC-based cavity-enhanced FTS. The measurements spanned the wavenumber range from 6270 $\mathrm{cm}^{-1}$ to 6410 $\mathrm{cm}^{-1}$ which covered lines from P(17) to R(22). The broad spectral bandwidth of the system allowed us to measure all the P branch lines simultaneously and then to measure all the R branch lines, eliminating systematic errors that may occur in cw-laser based step-scan systems, such as slow changes of pressure. First, we constructed an OFC-based spectrometer employing CEAS and FTS, and evaluated the detection sensitivity of the spectrometer. We calibrated the frequency axis following the procedure described in Ref.[35] and verified the removal of the ILS on low-pressure (10 Torr) line shapes. In Ref.[35], the authors reported precise line-shape measurements of transitions in the $3\nu_1+\nu_3$ band of $CO_2$, which required a line profile beyond the Voigt profile (VP) to model them within the experimental noise. Here, we present precise measurements of CO perturbed by Ar performed at 3 pressures: 100, 450 and 700 Torr. We performed VP and speed-dependent Voigt profile (SDVP) fits of the line profiles to derive collisional line-shape parameters. We discuss the uncertainty of retrieved line-shape parameters and propose some improvements for future line-shape studies.

## II. EXPERIMENTS

Our experimental setup is illustrated in FIG. 1(a). A mode-locked Er-doped fiber laser (Menlo System FC-1500) is used as the OFC. The repetition rate ($f_{\mathrm{rep}}$) of the OFC is 250 MHz, and the center wavelength is 1560 nm. We use output from Er-doped fiber amplifier, which has broadband spectral range of 1520−1670 nm at maximum pump laser power. The OFC beam passes through an electro-optic modulator (EOM) and couples into a high-finesse cavity. The cavity consists of two highly reflective mirrors with finesse of 21000 mounted in a vacuum chamber. The distance between the mirrors is 60 cm, which corresponds to free spectral range (FSR) of 250 MHz. The vacuum chamber is filled with a sample gas that is a CO-Ar mixture with CO concentration of 1000 ppm. To achieve simultaneous resonance of a high number of comb modes with cavity modes, we use a two-point Pound-Drever-Hall (PDH) locking technique [21, 22, 36]. The light reflected from the cavity is dispersed by a diffraction grating and two different regions of the spectrum are directed to separate detectors. The signals from the two detectors are used to generate error signals for $f_{\mathrm{rep}}$ and offset frequency ($f_0$) feedback loops. In addition, a phase lock of $f_{\mathrm{rep}}$ signal to an RF standard is established by a feedback control of a piezoelectric transducer (PZT) attached to one of cavity mirrors—the cavity length is stabilized to keep the $f_{\mathrm{rep}}$

DOI:10.1063/1674-0068/cjcp1911192 

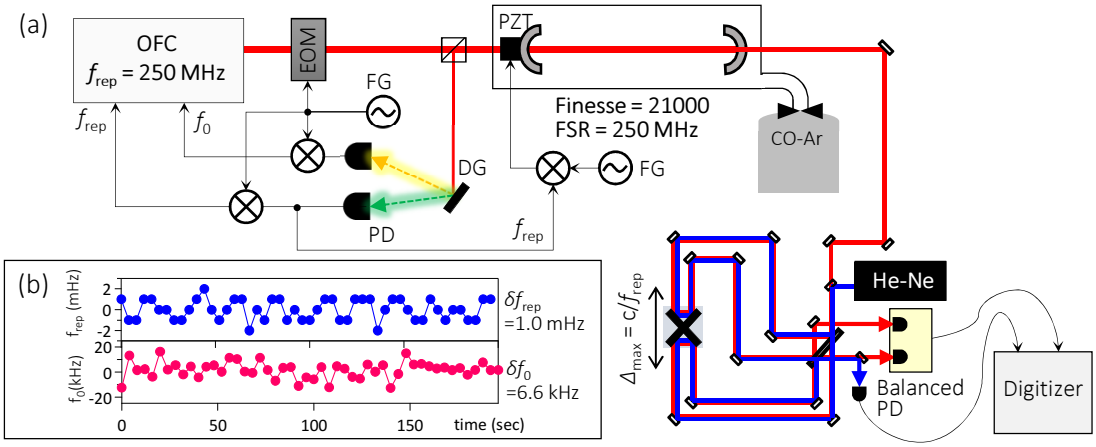


FIG. 1 (a) Experimental setup for comb-based CEAS and FTS. EOM-electro-optic modulator for two-point PDH lock, FG-function generator, DG-diffraction grating, PZT-piezoelectric transducer, PD-photo detector. (b) Frequency deviation of $f_{rep}$ (blue) and $f_0$ (red) during 50 times averaging in a measurement.

stable. We use the UTC(AOS) frequency standard as the RF reference for all function generators (FG) and frequency counters in this setup. UTC(AOS) realizes stabilities of $2\times10^{-13}$ in 1 s and $7.1\times10^{-16}$ in a day [37]. The $f_0$ signal is observed by an $f-2f$ interferometer, and $f_{rep}$ and $f_0$ are measured by a frequency counter during measurements. For the calibration of frequency axis of obtained spectra, we use averaged $f_{rep}$ and $f_0$ values from frequency counter measurements. FIG. 1(b) shows frequency deviations from averaged values of $f_{rep}$ and $f_0$ monitored during a measurement. The standard deviation of the $f_{rep}$ and $f_0$ were 1.0 mHz and 6.6 kHz, respectively. The slope of two-point PDH lock error signal is determined by cavity mode width, and it is broadened by contribution of many comb modes because the cavity dispersion inhibits simultaneous resonance between cavity and comb modes. The relatively large deviation of $f_0$ is considered to be caused by cross-talks between two servo loop for $f_{rep}$ and $f_0$ stabilizations, and drift of PDH error signal offset. Although the uncertainty of $f_{rep}$ is multiplied by mode number, approximately $10^6$ at near-infrared region, the frequency accuracy determined by comb modes is sufficiently high for the purpose of line shape measurement in Doppler limit. The light transmitted by the high-finesse cavity is introduced into a home-made FTS system. It consists of a standard Michelson interferometer with a double-sided retroreflector placed on a moving stage. The input beam is split and reflected back from both sides of the retroreflector, therefore the optical path difference ($\Delta_{max}$), *i.e.* the interferogram length, is 4 times the mechanical scan length. This arrangement greatly reduces the measurement time and the space taken by the setup. As a reference for the scan length of the interferometer, a stabilized He-Ne laser (wavelength of approximately 632.8 nm) was used, and the sampling interval was set to $\lambda_{HeNe}/2$. In an OFC-based FTS, $\Delta_{max}$ must be set to $c/f_{rep}$ to eliminate the effects of the ILS. Since $c/f_{rep}$=1.2 m, the mechanical scan length of the interferometer can be as short as 30 cm. The sampling points of the spectrum are evenly spaced by $c/\Delta_{max}$, which is equal to the comb mode interval. To get high density of spectral elements, especially in measurements at low pressures in which rovibrational lines are narrow, comb mode frequency is slightly changed to obtain an interleaved spectrum. In this work, at low pressure conditions, $f_{rep}$ was changed by 65 Hz to obtain the interleaved spectrum, which corresponds to a point spacing of 50 MHz in the optical region. The acquisition time for one interferogram was 4 s and the obtained spectra were integrated 50 times for each condition. Total measurement time was 200 s without interleaving and 17 min for interleaved spectra.

## III. RESULTS AND DISCUSSION

### A. Measured spectra and sensitivity

FIG. 2(a) displays transmission spectra of high-finesse cavity obtained at CO-Ar gas pressure of 100 Torr. Spectral range of the transmission depends on dispersion of cavity mirrors, cavity finesse and FSR, and comb mode width. The cavity dispersion includes both the molecular and mirror coatings' dispersion, thus depending on total pressure of samples. In contrast to comb mode structure, which has equal mode spacing over the whole emission spectrum, the FSR of a cavity varies with wavelength due to the cavity dispersion [20]. In our setup it limits the transmission range to about 100 $cm^{-1}$. The transmitted wavelength region can be selected by choosing the two-point PDH lock wavelengths. The spectra shown in red and blue in FIG. 2(a) are optimized for P and R branch measurements, respectively. The two maxima in each transmission spectra (6285 nm and 6350 nm for P branch, 6340

DOI:10.1063/1674-0068/cjcp1911192 

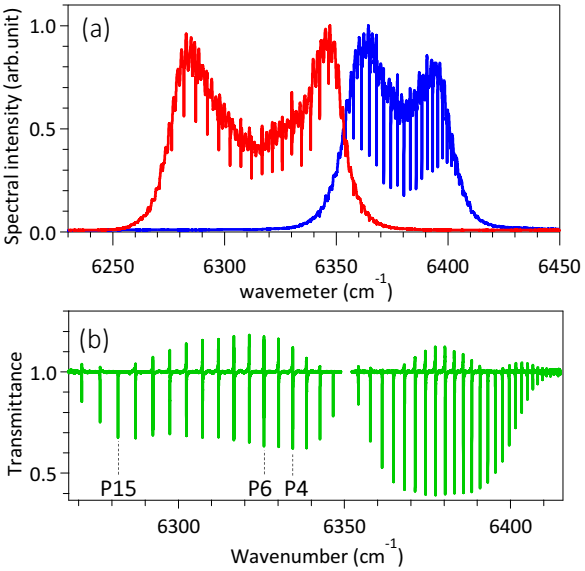


FIG. 2 (a) Cavity transmission spectra obtained by comb based FTS, and (b) normalized spectra of 0−3 band of CO. The pressure of CO-Ar mixture was 100 Torr, and 50 spectra were averaged in 200 s.

nm and 6395 nm for R branch) show the wavelengths used for feed back to $f_{\rm rep}$ and $f_0$ in the two-point PDH lock. In order to obtain baseline spectra for normalization, we introduced a reference $N_2$ gas with the same pressure as the CO-Ar gas into the cavity and measured the cavity transmission spectrum. The normalized spectra after background subtraction at 100 Torr are shown in FIG. 2(b). The normalization removed large fringes in the transmission spectrum (FIG. 2(a)), and the resulting spectrum achieved SNR up to 1200. The minimum detectable absorption calculated from the SNR and the effective path length of the cavity was $1.0 \times 10^{-9}$ cm$^{-1}$, and the minimum detectable absorption per spectral element for the range of P branch was $1.3 \times 10^{-10}$ cm$^{-1}$·Hz$^{-1/2}$. These values of minimum detectable absorption are similar to the ones reported previously for other OFC-based CEAS systems [23].

### B. Calibration of frequency axis and the influence of ILS

Calibration of the frequency axis in OFC-based FTS was performed following the methods introduced in Refs.[9, 35]. To acquire an ILS-free spectrum, the OFC interferogram is resampled at zero-crossings of He-Ne laser interferogram, resulting in sample spacing of $\lambda_{\rm HeNe}/2$, and it is cut to be the closest to the length of $c/f_{\rm rep}$. When an interferogram has a length of $\Delta_{\rm max}$, then without applying any window functions the spectrum obtained from a Fourier transform is given by the convolution of the real spectrum and the ILS($\omega$)=$\Delta_{\rm max}$sinc($\Delta_{\rm max}\omega$), where $\omega$ is the frequency detuned from the line center. FIG. 3 shows a numerical simulation: a convolution of the ILS with

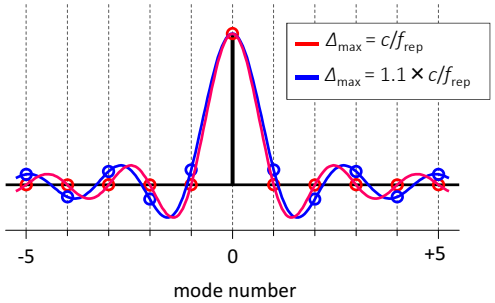


FIG. 3 Numerical simulation of the convolution of the ILS with a Dirac delta representing a comb mode. The ILS from interferogram with lengths $\Delta_{\rm max}$ of $c/f_{\rm rep}$ and $1.1\times c/f_{\rm rep}$ is shown in red and blue, respectively.

a Dirac delta representing a comb mode. In the case of $\Delta_{\rm max}$=$c/f_{\rm rep}$, the convolution always crosses zero at the other comb mode frequencies (red). On the other hand, the same convolution calculated for interferogram length of $1.1\times c/f_{\rm rep}$ (blue) has non-zero values at other mode frequencies and causes typical influence of ILS, such as broadening and ringing. The sampling density of interferograms does not provide enough high accuracy for the interferogram length determination. Due to this inaccuracy, the actual sampling frequency interval ($f_{\rm sample}$) in the resulting spectrum and $f_{\rm rep}$ cause a relative error of the order of $10^{-7}$.

In the optical frequency region, this difference is multiplied by comb mode number ($n$)—approximately $8\times10^5$—therefore, the mismatch between the comb mode frequency and the sampling point can be several tens of MHz, which is not negligible. A local agreement of both scales can be achieved by shifting the FTS frequency axis by $f_{\rm shift}$=$n\times(f_{\rm rep}-f_{\rm sample})$. The offset frequency of OFC, $f_0$, also introduces a mismatch because the FTS frequency scale offset is zero. The FTS scale must be also shifted according to the measured $f_0$ value. The spectrum with shifted scale is obtained by a Fourier transform of interferogram ($P(\Delta)$) multiplied by an exponential function containing shift frequencies:

$$S_{\rm FTS}(\nu) = \mathrm{abs}\left\{\mathrm{FFT}\left[P(\Delta)\exp\left(\frac{-i2\pi(f_0+f_{\rm shift})\Delta}{c}\right)\right]\right\} \quad (1)$$

In order to obtain an accurate value of $f_{\rm sample}$ for the calibration process, it is necessary to accurately determine the reference laser wavelength, $\lambda_{\rm HeNe}$. One useful method would be to stabilize the reference laser frequency using an OFC. Since a polarization-locked He-Ne laser was used in this work, which can exhibit slow drifts up to 1 MHz, we used transition frequencies given in Ref.[33] as the reference value of CO transition, and the value of $\lambda_{\rm HeNe}$ was derived so that the obtained transition frequencies matched.

FIG. 4(a) shows a normalized spectrum of the P6 line observed at 10 Torr with point spacing of 50 MHz

DOI:10.1063/1674-0068/cjcp1911192 

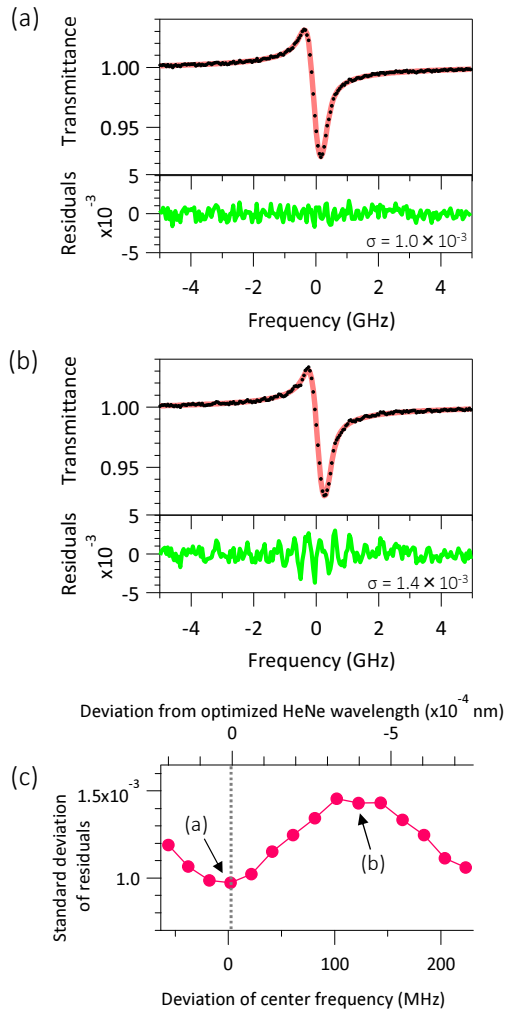


FIG. 4 (a) Calibrated experimental spectra of P6 line (black dots) using optimized $\lambda_{\mathrm{HeNe}}$. The VP fittings (red), residuals (green) is shown in the same plot, and residuals and the standard deviations ($\sigma$) are in bottom plot. (b) The same plots with (a) are shown for the same line calibrated using slightly different $\lambda_{\mathrm{HeNe}}$ value, optimized $\lambda_{\mathrm{HeNe}}$ of $4\times10^{-4}$ nm. (c) Trace of standard deviation of VP fitting for P6 lines obtained by changing $\lambda_{\mathrm{HeNe}}$ value. Upper and bottom horizontal axes show the $\lambda_{\mathrm{HeNe}}$ deviation from optimized wavelength and center frequency of P6 line in calibrated spectra, respectively.

obtained by interleaving (black). The frequency axis calibration was performed as described above. The line-shape function obtained by least-squares fitting of the VP is also shown in the same plot (red). We used cavity transmission equation [22] containing dispersion part of the molecular transition to describe the asymmetric line shape. Details of fitting functions are written in the next paragraph. In this pressure region, Doppler broadening is dominant and the line shape is well described by the VP. The full Doppler width was calculated from the room temperature and fixed to 442 MHz; the fitted collisional broadening was less than 10% of the Doppler width. Half-width at half maximum (HWHM) of the line is smaller than $f_{\mathrm{sample}}$, however, the bottom plot in FIG. 4(a) shows flat residuals and demonstrates that the influence of ILS is not present. The standard deviation ($\sigma$) values of the fit residuals with respect to the $\lambda_{\mathrm{HeNe}}$ value adopted in the calibration procedure are plotted in FIG. 4(c). Upper and lower horizontal axes show the deviation of $\lambda_{\mathrm{HeNe}}$ value and deviation of center frequency of P6 line after re-calibration with different $\lambda_{\mathrm{HeNe}}$, respectively. The smallest $\sigma$ was obtained with $\lambda_{\mathrm{HeNe}}$ that gives the correct transition frequency. The dependence of $\sigma$ on the $\lambda_{\mathrm{HeNe}}$ has the form of a sine function. FIG. 4(b) shows the calibrated spectrum, the fitted profile, and the residuals at the point where the residual becomes the largest in FIG. 4(c). The influence of ILS is clearly visible in the residuals as a ringing around the absorption line. When we add some deviation to the optimal $\lambda_{\mathrm{HeNe}}$ value, the offset frequency by which the FTS scale is shifted—$n\times(f_{\mathrm{rep}}-f_{\mathrm{sample}})$—is incorrect and this results in an inconsistency between the comb mode frequencies and the sampling points of the FTS spectrum. The plot of $\sigma$ values proves that the influence of ILS was successfully removed by the frequency calibration process.

### C. Fitting of line shapes and derivation of collisional parameters

Following the report by Foltynowicz *et al.* [22], the intensity of cavity transmission is written as:

$$\frac{I_t(\nu)}{I_0(\nu)} = \frac{T^2\mathrm{e}^{-2\delta(\nu)L}}{1-R^2\mathrm{e}^{-4\delta(\nu)L}-2R\mathrm{e}^{-2\delta(\nu)L}\cos[2\phi(\nu)L+\varphi(\nu)]} \quad (2)$$

where, $T$ and $R$ are intensity transmission and reflection coefficients of cavity mirrors, respectively, $L$ is the cavity length, $\varphi(\nu)$ is the round trip phase shift given by $2\pi\Delta\nu/\mathrm{FSR}$, where $\Delta\nu$ is the frequency detuning of comb modes from cavity resonant peak, called here the comb-cavity offset. Terms $\delta(\nu)$ and $\phi(\nu)$ are the frequency-dependent attenuation and phase shift of the electric field due to the intracavity sample. They are given by:

$$\delta(\nu) = \frac{Sn_{\mathrm{A}}}{2}\mathrm{Re}\chi(\nu) \quad (3)$$

$$\phi(\nu) = \frac{Sn_{\mathrm{A}}}{2}\mathrm{Im}\chi(\nu) \quad (4)$$

Here, $S$ is the molecular line strength in HITRAN unit of $\mathrm{cm}^{-1}\cdot\mathrm{molecule}^{-1}\cdot\mathrm{cm}^{-2}$, $n_{\mathrm{A}}$ is the density of absorbers ($\mathrm{molecules/cm}^3$), and $\chi(\nu)$ is the complex line-shape function. The asymmetric line shapes arise from the cosine term in Eq.(2). The molecular transitions change the refractive index, which can be interpreted as a local change of the FSR affecting the comb mode transmission intensity.

DOI:10.1063/1674-0068/cjcp1911192 

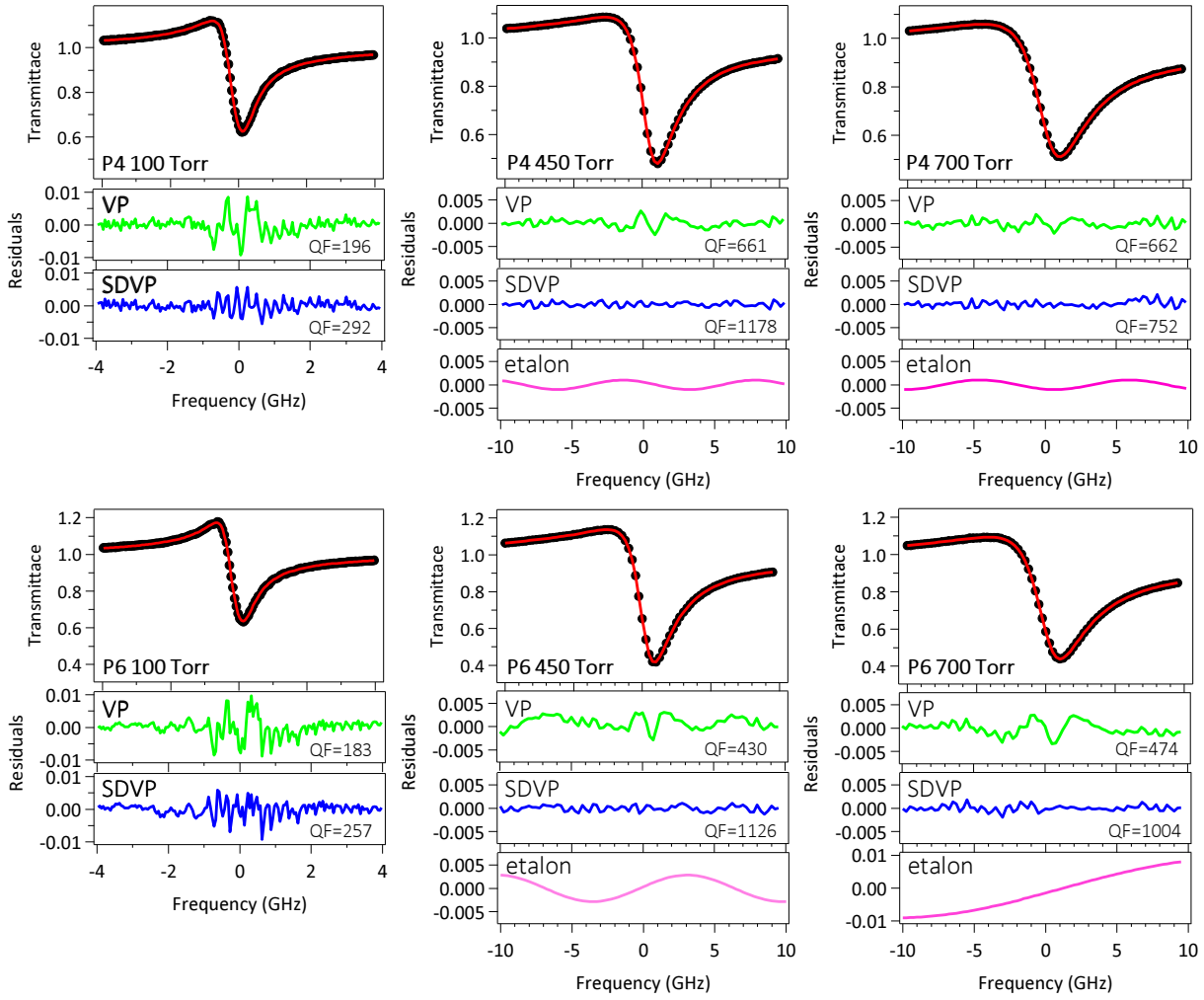


FIG. 5 Experimental (black) and fitted (red) line profile of P4 and P6 at 100, 450, and 700 Torr. Residuals of fitting with VP (green) and SDVP (blue), and the QF values are shown in lower parts. The fitted etalons (magenta) are shown under the residuals.

We analyzed the observed spectra by fitting Eq.(2) with an appropriate line-shape profile substituted for $\chi(\nu)$. It is well known that speed-dependent effects cannot be neglected in the CO line shapes [33, 38], therefore we used the SDVP [39] besides the VP to analyze the spectra. The speed dependence of pressure broadening in the SDVP was introduced using the quadratic approximation [40]:

$$\gamma_L(x) = \gamma_L B_w(x) = \gamma_L[1 + a_w(x^2 - 3/2)] \qquad (5)$$

where $x$ is the reduced absorber speed and $a_w$ quantifies the magnitude of the speed dependence relative to the speed-averaged pressure width, $\gamma_L$. The speed-dependence of collisional shift is small enough to be ignored thus the speed-dependent collisional shift $B_s(x)$ was fixed to one in our fits. At 100 Torr the spectral lines were measured at five different $f_{\rm rep}$ values to obtain 50 MHz point spacing after interleaving. At 450 and 700 Torr they were measured at a single $f_{\rm rep}$ value, corresponding to 250 MHz point spacing. The final spectra were obtained after applying the frequency axis calibration procedure described above. Single-line fits were performed on each pressure spectra using fit parameters of center frequency, line intensity, collisional line broadening, and comb-cavity offset $\Delta\nu(\nu)$ for the VP, and also of $a_w$ for the SDVP. In general, the comb-cavity offset depends on frequency but we assumed a constant value for the offset in the range of a single fit, because the influence of variation of $\Delta\nu(\nu)$ was not detectable within our SNR. The Doppler width was fixed to a value calculated from the room temperature during the measurement. Residual etalons in the baseline of normalized spectra were fitted out using sine functions.

FIG. 5 shows the experimental data of P4 and P6 lines at each pressure (black dots), fitted line profiles (red), residuals of VP (green), and SDVP fits (blue), and fitted etalon (magenta) for the lines at 450 Torr and 700 Torr. The quality factors (QFs) shown under the residual plots are calculated from the ratio of absorp-

DOI:10.1063/1674-0068/cjcp1911192 

TABLE I Line shape parameters derived from the SDVP fitting. The $\Delta_L$ and $\gamma_L$ are in units of $10^{-19}$ GHz·molecule$^{-1}$·cm$^3$, and the line positions is in MHz.

| | P4 | | | P6 | | |
|---|---|---|---|---|---|---|
| | $\nu_0$ | $\Delta_L$ | $\Gamma_L$ | $\nu_0$ | $\Delta_L$ | $\Gamma_L$ |
| This work | 189901443.1 (5.8) | −0.0863 (31) | 1.4023 (11) | 189642673.9 (2.1) | −0.0962 (14) | 1.288 (11) |
| CRDS [33] | 189901444.5 | −0.0882 | 1.403 | 189642678.8 | −0.10167 | 1.2568 |
| Diff | 1.5 MHz | −2.2% | 0.05% | −4.9 MHz | −5.4% | 2.5% |

tion peak to standard deviation of residuals. The residuals of VP fits show systematic w-shaped discrepancies due to the neglected speed dependence of broadening. The SDVP significantly improves residuals and better agreement for both lines at all pressures is obtained. This results show that the OFC-based cavity-enhanced Fourier-transform spectrometer allows for accurate line shape measurements exceeding the accuracy of the VP even in the case that line shapes have strong asymmetry. The center frequency at zero pressure ($\nu_0$), pressure shift ($\Delta_L$) and broadening ($\gamma_L$) coefficients of P4 and P6 lines were determined from the results of SDVP fitting at the three pressures. The pressure broadening and shift were assumed to be linear. Table I shows the derived line shape parameters. $\Delta_L$ and $\gamma_L$ are in units of $10^{-19}$ GHz·molecule$^{-1}$·cm$^3$ and the linear fit uncertainties are given in the parentheses. The table also shows a comparison with parameters given by the precise and accurate cw-laser CRDS measurements [33]. The differences in collisional pressure and broadening coefficients are both a few percent, and those in center frequency are a few MHz; all the parameters are in good agreement.

### D. Discussion: uncertainty of the line-shape parameters

In the line shapes in FIG. 5, as the FTS axis has been calibrated according to the procedure described above, the influence of ILS has been removed. Nonetheless, the residuals of P4 and P6 lines at 100 Torr show large discrepancies near the line center. FIG. 6 shows the P15 line obtained in the same measurement and with the same calibration. The P15 line has smaller asymmetry because the transition was close to one of the two-point lock wavelengths, and the SDVP fit residuals show smaller discrepancies and a higher QF value than that for P4 and P6 lines. This leads us to conclude that the larger fitting uncertainties of P4 and P6 lines are most likely caused by fluctuations of the cavity-comb offset during the measurement, as the lines with larger asymmetry have larger discrepancies. Asymmetric line shapes are due to the cosine part, which depends on the cavity-comb offset term as shown in Eq.(2), therefore, the comb-cavity offset fluctuation at larger absolute values has significant influence on the distortion of measured line shapes. In this case, the comb-cavity offsets of P4 and P6 were −7.4 kHz and −10.2 kHz, respectively, and P15 was −0.2 kHz. These cavity-comb offset fluctuations were most probably caused by the residual cross-talk between two servo loops stabilizing $f_{\rm rep}$ and $f_0$. Even in the measurement without interleaving, those fluctuations affected the measured line shapes. This decreases the accuracy of the determination of line shape parameters. To reduce the influence of those effects we can either limit the analysis to the low comb-cavity offset range or we can use low dispersion mirrors to limit this offset.

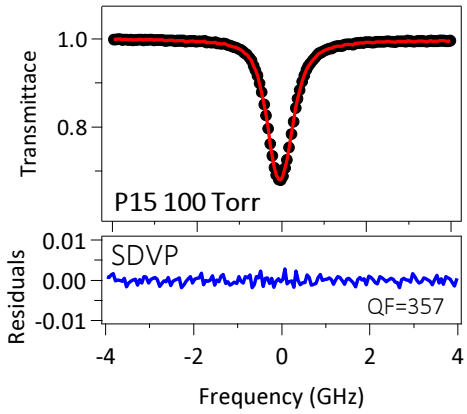


FIG. 6 Experimental data (black) of interleaved spectra of P15 observed at 100 Torr and fitted profile (red) and residuals (blue) with SDVP.

## IV. CONCLUSION

In conclusion, an OFC-based cavity-enhanced Fourier-transform spectrometer was constructed and it was proved that the system is valuable for line-shape studies. We adopted a high finesse cavity for the observation of second overtone band of CO and a highly sensitive measurement was performed with detectable absorption per spectral element of $1.3\times10^{-10}$ cm$^{-1}$·Hz$^{-1/2}$. The high resolution surpassing nominal resolution of FTS was demonstrated by applying the frequency calibration method introduced in Refs.[9, 35]. The influence of ILS was successfully removed and narrow spectral line shapes limited by Doppler broadening were observed with 50 MHz point spacing. A line-shape study was performed for P4 and P6 lines observed at several pressures. The observed

DOI:10.1063/1674-0068/cjcp1911192 

spectra provided accurate line-shape profiles beyond the VP. Line-shape parameters were determined from the SDVP fits, which showed good agreement with the results of precise cw-laser CRDS measurements.

With a step-scanned cw-laser CRDS setup, it is in practice difficult to acquire spectral data of a large number of lines, but our system enabled us to acquire 40 lines in P and R branches in a short amount of time and with high sensitivity. Moreover, accurate narrow line shapes that conventional FTIR cannot be measured due to that the ILS was observable with our system. Based on the discussion about uncertainty of obtained line shapes mentioned above, we estimate that the precision of the line shape parameters will be improved by introducing low dispersion mirrors. In the ongoing experiments, we will derive the spectroscopic parameters of a large number of rovibrational lines, and soon they will be available for the application in various fields such as astronomy and atmospheric science.

## V. ACKNOWLEDGMENTS

This work was supported by National Science Center, Poland Projects No.2016/23/B/ST2/00730, 2016/21/N/ST2/00334. Grzegorz Kowzan was supported by National Science Center, Poland Scholarship No.2017/24/T/ST2/00242.

[1] T. Udem, J. Reichert, R. Holzwarth, and T. W. Hänsch, Opt. Lett. **24**, 881 (1999).
[2] D. J. Jones, S. A. Diddams, J. K. Ranka, A. Stentz, R. S. Windeler, J. L. Hall, and S. T. Cundiff, Science **288**, 635 (2000).
[3] S. A. Diddams, L. Hollberg, and V. Mbele, Nature **445**, 627 (2007).
[4] M. J. Thorpe, D. Balslev-Clausen, M. S. Kirchner, and J. Ye, Opt. Express **16**, 2387 (2008).
[5] F. Keilmann, C. Gohle, and R. Holzwarth, Opt. Lett. **29**, 1542 (2004).
[6] I. Coddington, W. C. Swann, and N. R. Newbury, Phys. Rev. Lett. **100**, 013902 (2008).
[7] I. Coddington, N. Newbury, and W. Swann, Optica **3**, 414 (2016).
[8] J. Mandon, G. Guelachvili, and N. Picqué, Nature Photon. **3**, 99 (2009).
[9] P. Masłowski, K. F. Lee, A. C. Johansson, A. Khodabakhsh, G. Kowzan, L. Rutkowski, A. A. Mills, C. Mohr, J. Jiang, M. E. Fermann, and A. Foltynowicz, Phys. Rev. A **93**, 021802(R) (2016).
[10] B. Spaun, P. B. Changala, D. Patterson, B. J. Bjork, O. H. Heckl, J. M. Doyle, and J. Ye, Nature **26**, 517 (2016).
[11] P. B. Changala, M. L. Weichman, K. F. Lee, M. E. Fermann, and J. Ye, Science **363**, 49 (2019).
[12] A. Nishiyama, S. Yoshida, Y. Nakajima, H. Sasada, K. Nakagawa, A. Onae, and K. Minoshima, Opt. Express **24**, 25894 (2016).
[13] A. Nishiyama, Y. Nakajima, K. Nakagawa, and K. Minoshima, Opt. Express **26**, 8957 (2018).
[14] G. Ycas, F. R. Giorgetta, K. C. Cossel, E. M. Waxman, E. Baumann, N. R. Newbury, and I. Coddington, Optica **6**, 165 (2019).
[15] P. R. Griffiths and J. A. de Haseth, *Fourier Transform Infrared Spectrometry*, Hoboken, NJ: Wiley, (2007).
[16] M. J. Thorpe, K. D. Moll, R. J. Jones, B. Safdi, and J. Ye, Science **311**, 1595 (2006).
[17] A. C. Johansson, L. Rutkowski, A. Filipsson, T. Hausmaninger, G. Zhao, O. Axner, and A. Foltynowicz, Opt. Express **26**, 20633 (2018).
[18] G. Kowzan, D. Charczun, A. Cygan, R. S. Trawiński, D. Lisak, and P. Masłowski, Sci. Rep. **9**, 8206 (2019).
[19] C. Gohle, B. Stein, A. Schliesser, T. Udem, and T. W. Hänsch, Phys. Rec. Lett. **99**, 263902 (2007).
[20] M. J. Thorpe and L. Ye, Appl. Phys. B **91**, 397 (2008).
[21] A. Foltynowicz, T. Ban, P. Masłowski, F. Adler, and J. Ye, Phy. Rev. Lett. **107**, 233002 (2011).
[22] A. Foltynowicz, P. Masłowski, A. J. Fleisher, B. J. Bjork, and J. Ye, Appl. Phys. B **110**, 163 (2013).
[23] A. Foltynowicz, P. Masłowski, T. Ban, F. Adler, K. C. Cossel, T. C. Briles, and J. Ye, Faraday Discuss **150**, 23 (2011).
[24] I. E. Gordon, et al., J. Quant. Spectrosc. Radiat. Transf. **203**, 3 (2017).
[25] P. J. Crutzen, L. E. Heidt, J. P. Krasnec, W. H. Pollock, and W. Seiler, Nature **282**, 253 (1979).
[26] T. M. Dame, D. Hartmann, and P. Thaddeus, Astrophys. J. **547**, 792 (2001).
[27] R. A. Thomas, P. Claude, and U. K. Christoph, Astrophys. J. **165**, 618 (2006).
[28] J. P. Bouanich, F. Rachet, and A. Valentin, J. Mol. Spectrosc. **178**, 157 (1996).
[29] R. Wehr, A. Vitcu, R. Ciuryło, F. Thibault, J. R. Drummond, and A. D. May, Phys. Rev. A **66**, 062502 (2002).
[30] R. Wehr, R. Ciuryło, A. Vitcu, F. Thibault, J. R. Drummond, and A. D. May, J. Mol. Spectrosc. **235**, 54 (2006).
[31] R. Wehr, A. Vitcu, F. Thibault, J. R. Drummond, and A. D. May, J. Mol. Spectrosc. **235**, 69 (2006).
[32] J. P. Bouanich and C. Haeusler, J. Quant. Spectrosc. Radiat. Transf. **12**, 695 (1972).
[33] G. Kowzan, K. Stec, M. Zaborowski, S. Wójtewicz, A. Cygan, D. Lisak, P. Masłowski, and R. S. Trawiński, J. Quant. Spectrosc. Radiat. Transf. **191**, 46 (2017).
[34] N. H. Ngo. H. Lin, J. T. Hodges, and H. Tran, J. Quant. Spectrosc. Radiat. Transf. **203**, 325 (2017).
[35] L. Rutkowski, P. Masłowski, A. C. Johansson, A. Khodabakhsh, and A. Foltynowicz, J. Quant. Spectrosc. Radiat. Transf. **204**, 63 (2018).
[36] R. J. Jones and J. C. Diels, Phys. Rev. Lett. **86**, 3288 (2001).
[37] Ł. Śliwczyński, P. Krehlik, A. Czubla, Ł. Buczek, and M. Lipiński, Metrologia **50**, 133 (2013).
[38] S. Wójtewicz, K. Stec, P. Masłowski, A. Cygan, D. Lisak, R. S. Trawiński, and R. Ciuryło, J. Quant. Spectrosc. Radiat. Transf. **130**, 191 (2013).
[39] P. R. Berman, J. Quant. Spectrosc. Radiat. Transf. **12**, 1331 (1972).
[40] D. Priem, F. Rohart, J. M. Colmont, G. Wlodarczak, and J. P. Bouanich, J. Mol. Spectrosc. **517/518**, 435 (2000).

DOI:10.1063/1674-0068/cjcp1911192 